Analysis of the Wave Modes for Super-High Frequency SAW Devices on the SiO_2/IDT/$LiNbO_3$ Structure

Danhua Li, Changjian Zhou
School of Microelectronics
South China University of Technology
Guangzhou, China
zhoucj@scut.edu.cn

Salahuddin Raju, Mansun Chan
Department of Electronic and Computer Engineering
The Hong Kong University of Science and Technology
Kowloon, Hong Kong

***Abstract*—We study the influence of wave propagation direction on the SAW modes excitation and their characteristics in the SiO_2/IDT/128°Y-cut $LiNbO_3$ structures. The three-dimensional finite element method analysis reveals that the multilayer structure can support the Love wave, Rayleigh wave, Sezawa wave, 1st Love wave, and 2nd Rayleigh wave. Consistent with the measured result of the super-high frequency (2-10 GHz) SAW devices, the Love wave mode is coupled with the Rayleigh wave mode. Meanwhile, because of the effect of the electrode, symmetric and antisymmetric modes of the Rayleigh wave and Sezawa wave appear simultaneously. This work guides further optimization of the device at super-high frequency.**

Keywords—surface acoustic wave (SAW), lithium niobate, mode analysis, super high frequency (SHF)

I. INTRODUCTION

The temperature-compensated structure composed of $LiNbO_3$(LN) single crystal substrate and SiO_2 layer has been reported in many articles [1]-[6]. By far, because of the dispersive effect in the multilayer structure, many articles have reported shear horizontal wave, leaky wave, Rayleigh wave, and other wave modes analysis below 2 GHz. However, concerning the multilayered structure incorporating LN substrate for super-high frequency device development, there is still little information on the wave modes excitation and mode coupling effect due to the complex dispersive characteristics of the layered structure. In this work, the mode characteristics with different propagation directions of super-high frequency SAW devices are investigated.

II. SIMULATION

A multilayer structure of SiO_2/128°Y-cut single crystal LN is employed in this work for the high K_{eff}^2 and low TCF. To study the propagation characteristic in the SiO_2/128°Y-cut LN multilayer structure, we construct a 3D FEM model of SiO_2/IDT/128°Y-LN multilayer structure with 400 nm wavelength(λ). To reduce the complexity of the simulation, a unit cell of SiO_2/IDT/LN multilayer structure with one wavelength wide and one wavelength length is shown in Fig.1(a). A perfectly matched layer (PML) with one wavelength height is added to the bottom of the substrate to prevent wave reflection from the finite depth substrate. As the mechanical displacement of SAW is mostly confined to the range of 1 to 2 wavelengths from the device surface, the thickness of the substrate is set to 5λ for computation effectiveness. The thickness of the SiO_2 layer on the LN substrate is 300 nm. 30 nm thick Au electrodes are inserted between the LN substrate and SiO_2 layer, with the metallization ratio of 1. The structural and electrical boundary conditions are as follows: the lower boundary is fixed, the right electrode is grounded and a terminal (1V) is applied to the left electrode, all the sides are set as the periodic boundary condition.

Because of the symmetry of the 128°Y-LN single crystal material, we only study the influence of the propagation direction with an angle of 0-90° from the x-axis of the LN on the mode excitation through eigenfrequency study and frequency domain. Eigenfrequency study gives the edges of the stopband. One of the edges is a symmetric mode for which electrodes deform symmetric about its centerline, and the other edge is an antisymmetric mode for which electrodes deformation is antisymmetric. The simulated admittances and mode shapes are shown in Fig.2. It can be found that the multilayer structure with different propagation directions can support five modes consisting of Love wave(L_0), Rayleigh wave(R_0), Sezawa wave(R_1), 1st Love wave(L_1), 2nd Rayleigh wave(R_2). Because the device with propagation along the 90° directrion has less spurious mode and higher K_{eff}^2 (Fig.2(b)), we further study the influence of LN thickness on mode characteristics in this propagation direction, and compare it with the mode characteristics in the 0° direction, as shown in

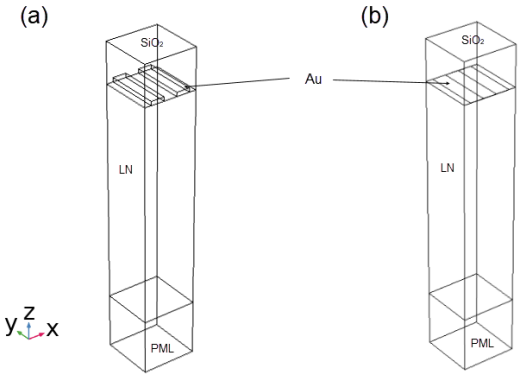

Fig.1. Schematic of a unit cell of SAW device based on SiO_2/IDT/LN structure (a) with 30 nm thick electrodes and (b) neglecting the thickness of electrodes

Fig.3. Fig.3(a) shows the velocity dispersion curves of the first three modes versus normalized SiO_2 thickness Kh_{SiO_2} in the SiO_2/128°YX-LN layered structures, where h_{SiO_2} is the thickness of SiO_2 layer, and $K=2\pi/\lambda$. It can be seen that the velocities of Love wave and Rayleigh wave are so close. Therefore, the influence of this phenomenon is studied. The simulated admittance property of the device with 2000 nm wavelength is shown in Fig.4(a). It can be seen that there is only one resonance peak around 2 GHz and the mode shape is shown in the inset of Fig.4(a). Most of the energy is concentrated on the surface for this wave mode. Fig.4(b) shows the particle displacement distribution along the X-axis.

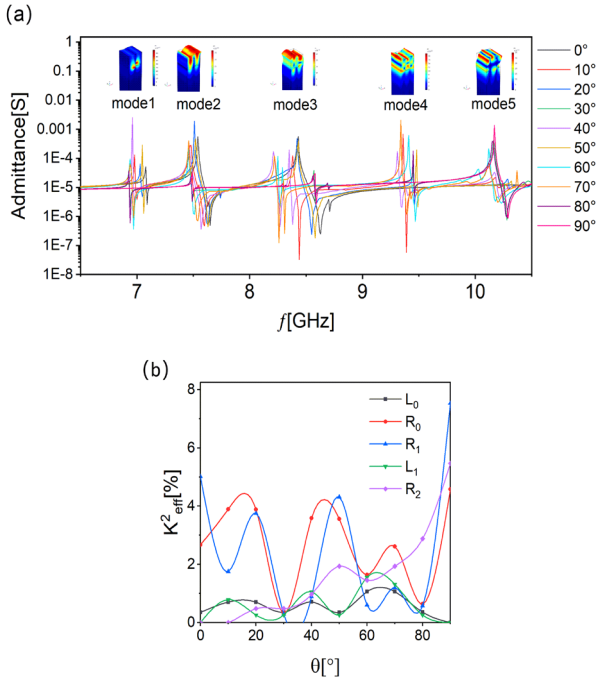

Fig.2. (a) The simulated admittance and (b) the simulated K^2_{eff} for 400 nm wavelength device with different propagation directions.

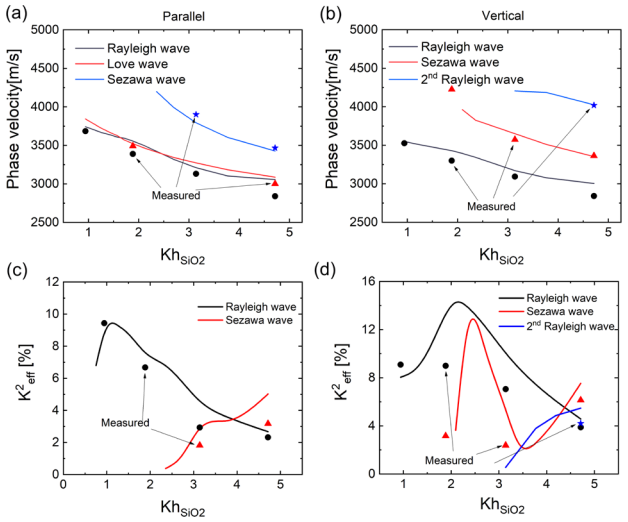

Fig.3. The simulated and experimental phase velocity and K^2_{eff} for the device with propagation direction along 0° and 90° direction.

X, Y, and Z components are the particle displacement components that are parallel to the X-, Y-, and Z-axis of the global coordinate system. Note that the displacements have been normalized relative to the largest of these three displacement components. It can be seen that the three displacement components distribution is periodic which means that the mode propagates along the X-direction. Besides, the X and Y displacement component is much higher than the Y displacement component. Therefore, the mode around 2 GHz is Rayleigh wave, and Love wave is suppressed. However, compared with the conventional Rayleigh wave, the displacement components in the Y direction does not approximately equal to zero, which shows that even Love wave mode is suppressed, the coupling effect remains.

Fig.3(b) shows the velocity dispersion curves of the first three modes in the SiO_2/128°Y90°X-LN layered structures. It can be seen that the first three modes are Rayleigh wave, Sezawa wave, and 2nd Rayleigh wave, which means that the multilayer structure propagating along the 90° direction has higher-order mode. However, the velocities of the same mode are lower than those propagating in the 0° direction.

Fig.3(c) and (d) are the K^2_{eff} dispersion curves for the device with propagation directions along 0° and 90°. Because the Love wave is suppressed in the SiO_2/IDT/128°YX-LN structure, Fig.3(c) only shows the K^2_{eff} of Rayleigh wave and Sezawa wave. The result shows that the device with propagation direction along 90° direction can obtain the higher K^2_{eff}.

III. Experiment

In this work, a commercial 128° Y-cut single-crystal LN wafer is employed as a piezoelectric substrate. Firstly, the ZEP 520A EBL photoresist was spin coated onto the substrate yielding an approxmate100 nm thick layer, followed by soft baked at 180℃ for 30 min. As the LN substrate is nonconductive and prone to severe charging under an electron beam, a 10 nm thick Cr layer was deposited on top of the photoresist. The electron beam lithography with an exposure dose of 130 $\mu C/cm^2$is performed to define the IDTs pattern. The IDTs patterns are either parallel or vertical to the main cut of the substrate. Then, Au/Ti(30 nm/5 nm) is deposited by e-beam evaporation and the IDTs metals were formed after the lift-off process. Finally, the 300 nm SiO_2 is deposited by plasma-enhanced chemical vapor deposition for

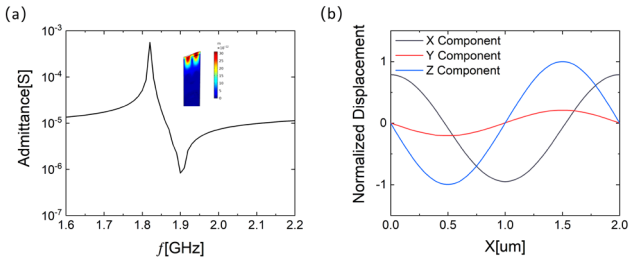

Fig.4. (a) The simulated admittance properties and (b) particle displacement distribution of the mode on SiO_2/IDT/128°YX-LN for 2000 nm wavelength. The mode shape is shown on the inset.

capping of the IDTs, which is a low-temperature process to ensure the stability of the deposited electrodes. Fig.5 shows the pictures of successfully fabricated SAW devices with very fine IDTs. The optical microscope images show the fabricated one-port and two-port IDTs (Fig.5(a)) and the magnified part of the two-port IDTs with a 500 nm finger width (Fig.5(b)). Fig.5(c)–(f) are the SEM images of SAW IDTs with finger widths from 100 nm to 500 nm. The results show that the IDTs have smooth edges and the metallization ratio (MR) is about 0.5.

An Agilent E8361A vector network analyzer is used to measure S-parameters, and the frequency characteristics of SAW device are studied. Fig.6 shows the measured S_{11} spectra of the SAW devices with parallel and vertical IDTs of 400-2000 nm wavelengths. In general, the resonance frequencies of the fabricated devices are in the range of 2-10 GHz. Comparing the properties of SAW devices with two kinds of IDTs, the device with parallel IDTs has a higher resonance frequency than that with vertical IDTs for the same mode, which is the same as predicted by simulation.

For the SAW devices with parallel IDTs, the three resonance peaks observed for devices with 400nm and 1000 nm wavelengths are Rayleigh wave, Love wave, and Sezawa wave respectively, although the first two modes are very close for the device with 1000 nm wavelength (Fig.6(c)). Whereas, there is only one resonance peak around 5.3GHz for the devices with 600 nm wavelength, and there is also only one mode around 2GHz for the devices with 2000 nm wavelengths, which is because the velocities of Love wave mode are so close to the velocities of Rayleigh wave mode that one of Love wave is suppressed.

The SAW devices with vertical IDTs show 2 to 4 resonance peaks. Combined with the analysis above, the three resonance peaks of SAW devices with 400nm wavelength (Fig.6(a)) are Rayleigh wave, Sezawa wave, and R_2 respectively. As for the devices with 600 nm wavelength and 1000 nm wavelength, there are 4 peaks. The first and the fourth resonance peaks for the device with 600 nm wavelength in Fig.6(b) are Rayleigh wave and leaky wave whose velocity is higher than that of the slow shear velocity of LN substrate (~4079m/s)[7]. Meanwhile, the third and the fourth resonance peaks for the device with 1000 nm wavelength (Fig.6(c)) are Sezawa wave and leaky wave, respectively. However, the remaining two resonance peaks of these two devices with 600 nm and 1000 nm wavelengths are inconsistent with the numerical calculation results. Then, the remaining two mode shapes are further investigated through frequency domain study and eigenfrequency study. The admittance spectrum of these two devices is shown by the black line in Fig.7. It can be observed that the remaining two resonance peaks for the device with 600 nm wavelength coincide well with the symmetric mode and antisymmetric mode of Sezawa wave as shown in Fig.7(a). Similarly, the first and the second resonance peaks for the device with 1000 nm wavelength are the antisymmetric and the symmetric modes of Rayleigh wave as shown in Fig.7(b). Besides, the propagation characteristic of the model neglecting the

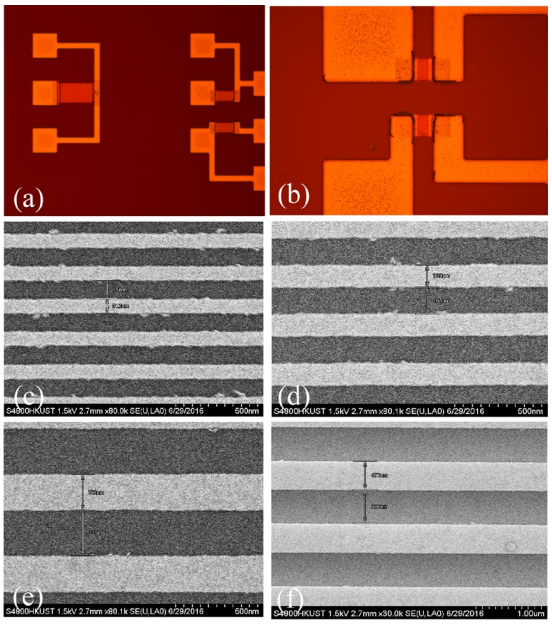

Fig.5. (a) Optical picture of the fabricated IDTs and (b) magnified part of the two-port IDTs with a 500 nm finger width; SEM pictures of IDTs of (c) 100 nm (d) 150 nm (e) 250 nm (f) 500 nm linewidth.

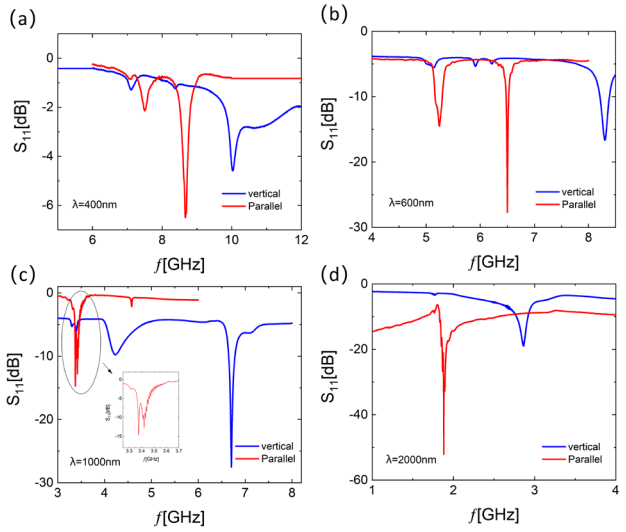

Fig.6. S_{11} spectra of the fabricated two-port SAW device with parallel and vertical IDTs of (a) 400 nm, (b) 600 nm, (c) 1000 nm, and (d) 2000 nm wavelength. The inset in (c) is the magnified part of the S_{11} spectra of the SAW device with parallel IDTs at around 3.4 GHz.

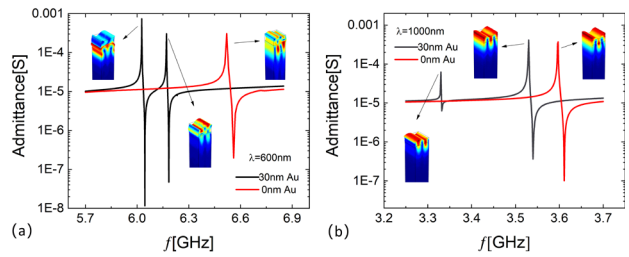

Fig.7. The comparison of the admittance on SiO_2/IDT/128°Y90°X-LN with 30 nm thick electrodes and ignoring the thickness of electrodes for (a) 600 nm wavelength and (b) 1000 nm wavelength.

thickness of electrodes shown in Fig.1(b) is investigated through a frequency-domain study. The parameters used in this model are the same as those used in the previous model except for the thickness of electrodes. Fig.7 shows the comparison of the admittance of the SAW devices with 30 nm thick electrodes and ignoring the thickness of electrodes for 600 nm and 1000 nm wavelength. It can be seen that there is only one mode for the device with neglecting electrode thickness. Therefore, the simultaneous appearance of symmetric mode and the antisymmetric mode is due to the loading effect of the electrodes, especially mass loading. Furthermore, as the mass loading effect of the electrodes, the resonance frequency of the devices with ignoring electrode thickness is higher than those with 30 nm Au electrodes, especially in the super-high frequency range. The two resonance peaks for the device with 2000 nm wavelength in Fig.6(d) are Rayleigh wave and leaky wave, respectively.

Moreover, it can be found that the return loss of Rayleigh wave and Sezawa wave in SAW devices with parallel IDTs is smaller. However, the return loss of higher-order modes in the SAW devices with vertical IDTs is smaller than that of other modes.

Besides, other essential performance metrics such as the phase velocity and K_{eff}^2 can be obtained from the S parameter. The experimental velocity and K_{eff}^2 are marked in the form of scattered points in Fig.3. The experimental measurement is in agreement with the simulation predictions. Actually, there are still deviations between the measured and the simulated performance parameters. The reason is that the boundary conditions and material parameters of the simulation are not exactly the same as those of the fabricated devices, especially for the PECVD SiO_2. In addition, a very fine IDTs is used in the SAW device to obtain super-high frequency, therefore a small deviation of the linewidth of IDTs will have a great impact on the metallization ratio and the resultant resonance frequency. In Fig.3, it can be seen that the R_2 mode propagating along the 90° direction of the 400 nm wavelength device exhibits the highest frequency of 10.03 GHz and extracted K_{eff}^2 of 4.2%.

IV. Conclusions

This work reports that super-high frequency SAW devices with SiO_2/IDT/128°Y-LN structure can support a total of 5 modes, including L_0, R_0, R_1, L_1, R_2 modes. In the propagation of the x-axis, the Love wave mode is coupled with Rayleigh wave mode, resulting in the Love wave being suppressed. In the propagation of the 90° direction, because of the effect of electrodes, symmetric mode and antisymmetric mode appear simultaneously. Compared with the SAW devices with parallel IDTs, the return loss of higer-order modes in SAW devices with vertical IDTs is smaller. Moreover, as for the 400 nm SAW resonator, the R_2 mode propagating along the 90° direction shows a high frequency of over 10 GHz and an extracted K_{eff}^2 of 4.2%, which is very promising for future high frequency SAW device applications.

References

[1] C. Zhou, Y. Yang, H. Cai, T. L. Ren, M. Chan, and C. Y. Yang, "Temperature-compensated high-frequency surface acoustic wave device," IEEE Electron Device Lett., vol. 34, no. 12, pp. 1572–1574, Dec. 2013.

[2] S. Raju, C. Zhou, B. Li, and M. Chan, "Temperature compensated super-high-frequency (2-8 GHz) surface acoustic wave devices," in 2017 International Symposium on VLSI Technology, Systems and Application, (VLSI-TSA), Hsinchu, Taiwan, Apr. 24-27, 2017, pp. 1–2.

[3] K. Yamanouchi and T. Ishii, "High temperature stable acoustic surface wave substrates of $SiO_2/LiNbO_3$ structure with super high coupling," Japanese J. Appl. Physics, Part 1 Regul. Pap. Short Notes Rev. Pap., vol. 41, no. 5B, pp. 3480–3482, May. 2002.

[4] R. Goto, H. Nakamura, and K. Y. Hashimoto, 'Spurious free TC-SAW duplexer using the $SiO_2/LiNbO_3$ structure', in IEEE International Ultrasonics Symposium. (IUS), 2019, pp. 2075–2078.

[5] M. S. Patel, K. Bhattacharjee, J. Reed, and S. Zhgoon, 'Temperature compensation of longitudinal leaky SAW with silicon dioxide overlay', in IEEE International Ultrasonics Symposium. (IUS), 2008, pp. 1006–1010.

[6] M. Mimura, D. Ajima, C. Konoma, 'Mitigation of High Frequency Spurious Responses in Rayleigh SAW Resonators on $LiNbO_3$ Substrate', in IEEE International Ultrasonics Symposium. (IUS), 2019, pp. 679–682.

[7] D. Cullen, G. Meltz, and T. Grudkowski, "Surface and interface acoustic waves in SiO_2/YX-$LiNbO_3$," Appl. Phys. Lett., vol. 44, no. 2, pp. 182–184, Nov. 1984.